Applied Catalysis B: Environmental 205 (2017) 189–200

Contents lists available at ScienceDirect

Applied Catalysis B: Environmental

journal homepage: www.elsevier.com/locate/apcatb

Investigation of competitive COS and HCN hydrolysis reactions upon an industrial catalyst: Langmuir-Hinshelwood kinetics modeling

David Chiche*, Jean-Marc Schweitzer

IFP Energies nouvelles, Rond-point de l'échangeur de Solaize, BP 3, 69360 Solaize, France

ARTICLE INFO

Article history:
Received 7 September 2016
Received in revised form
24 November 2016
Accepted 1 December 2016
Available online 5 December 2016

Keywords:
Synthesis gas
Purification
Kinetics modeling
Catalytic conversion
Titania

ABSTRACT

Distinct and simultaneous COS and HCN hydrolysis reactions over an industrial TiO_2 based catalyst were extensively studied in this work in the scope of synthesis gas purification applications. 144 experiments were carried out, including 92 experiments that allowed to achieve partial conversion rates and showed reaction kinetics sensitivity to operating parameters. Significant crossed influences were evidenced between both COS and HCN hydrolysis reactions. The concomitant occurrence of both reactions showed to detrimentally affect each other upon COS and HCN conversion rates, and therefore upon kinetic rates. This was explained through a competitive adsorption of HCN and COS reactants upon catalyst surface active sites. Inhibition of catalytic activity by the presence of NH_3 and H_2O was also evidenced and explained through competitive adsorption phenomena. For the operating conditions ranges explored, H_2S and CO_2 had no sensitive impact on the kinetics of the COS and HCN hydrolysis reactions. However, the moderate impact of CO_2 upon COS and HCN conversion rates might be explained by the large CO_2 excess compared to COS and HCN levels. A reaction model has been fully developed considering hydrodynamic, external mass transfer and intra particle diffusion limitations, and Langmuir-Hinshelwood reaction mechanisms for both COS and HCN hydrolysis reactions. Langmuir-Hinshelwood kinetic rate laws were indeed considered to account for the detrimental effect of gaseous species upon COS and HCN conversion kinetic rates, through competitive adsorption upon catalyst active sites of COS, HCN, H_2O, and NH_3. Collected kinetic data as a function of reactor size, gas residence time, temperature and reactants partial pressures were used to validate and fit kinetic and adsorption constants. Very good agreement was achieved between experimental and calculated COS and HCN conversion rates from the model developed, that allowed complete validation of the Langmuir-Hinshelwood based modeling. The coupled hydrodynamic-reaction model also constitutes a complete industrial reactor model taking into account all the potential limitations, and can be used as a powerful predicting tool for industrial process design, *i.e.* fully usable for industrial process scale-up and optimization purposes.

Abbreviations: A_p (m^2), particle surface area; α_i, thermodynamic parameter; β_i, thermodynamic parameter; T (K), temperature; b_{COS} (bar^{-1}), COS adsorption constant; b_{HCN} (bar^{-1}), HCN adsorption constant; b_{NH_3} (bar^{-1}), NH_3 adsorption constant; b_{H_2O} (bar^{-1}), H_2O adsorption constant; C_i^g ($mol\,m^{-3}$), gas concentration of compound i; C_i^p ($mol\,m^{-3}$), particle concentration of compound i; D_{ax}^g ($m^2\,s^{-1}$), gas axial dispersion coefficient; $D_{eff,i}$ ($m^2\,s^{-1}$), effective diffusion coefficient; d_p (m), particle diameter; D_m ($m^2\,s^{-1}$), molecular diffusion coefficient; E_1 ($J\,mol^{-1}$), activation energy of reaction 1; E_2 ($J\,mol^{-1}$), activation energy of reaction 2; k_1 (SI), kinetic constant of reaction 1; k_2 (SI), kinetic constant of reaction 2; k_{gs} ($m\,s^{-1}$), gas-solid mass transfer coefficient; $K_{eq,i}$, i^{th} thermodynamic constant; L_c (m), particle characteristic length; m_T, Thiele modulus; P_{COS} (bar), COS partial pressure; P_{CO_2} (bar), CO_2 partial pressure; P_{H_2S} (bar), H_2S partial pressure; P_{HCN} (bar), HCN partial pressure; P_{CO} (bar), CO partial pressure; P_{H_2O} (bar), H_2O partial pressure; P_t (bar), total pressure; Re, Reynolds number; r_1 ($mol\,s^{-1}\,kg^{-1}$), reaction rate of reaction 1; r_2 ($mol\,s^{-1}\,kg^{-1}$), reaction rate of reaction 2; R ($J\,mol^{-1}\,K^{-1}$), ideal gas constant; r (m), radius coordinate; R_p (m), particle radius; Sc, Schmidt number; Sh, Sherwood number; V_p (m^3), particle volume; v_{sg} ($m\,s^{-1}$), superficial gas velocity; z (m), reactor elevation; ΔH_{COS} (bar^{-1}), COS adsorption enthalpy; ΔH_{HCN} (bar^{-1}), HCN adsorption enthalpy; ΔH_{NH_3} (bar^{-1}), NH_3 adsorption enthalpy; ΔH_{H_2O} (bar^{-1}), H_2O adsorption enthalpy; ε_g, gas holdup; ε_s, solid holdup; ε_p, particle porosity; δ (m), film thickness; $\mu_{i,j}$, stoichiometric coefficient; ρ_g ($kg\,m^{-3}$), gas density; ρ_s ($kg\,m^{-3}$), solid density; τ, residence time; τ_p, particle tortuosity.

* Corresponding author.
E-mail address: david.chiche@ifpen.fr (D. Chiche).

http://dx.doi.org/10.1016/j.apcatb.2016.12.002
0926-3373/

1. Introduction

To protect the environment and preserve natural resources, a more diverse energy mix is essential, especially in the transportation industry. As the only liquid fuels that can be used to supplement fossil based transportation fuels, biofuels play a major role in the diversification process.

Some research is currently focusing on the development of second-generation biofuels that can be made from non-edible, ligno-cellulosic materials derived from wood, straw, forest wastes, and dedicated crops [1,2]. By using the non-edible part of plants, second-generation biofuels are expected to enable to meet growing biofuel needs without competing with food production. In addition, they can use raw materials that are in abundant supply and deliver an interesting environmental performance. Second-generation biofuels can be produced from biochemical and thermochemical routes. Especially, as shown in Fig. 1, thermochemical conversion consists in the gasification of carbonaceous feedstocks under partially oxidizing atmosphere into a synthesis gas (or syngas) composed of a CO-H_2 mixture [3]. After multiple gas conditioning steps aimed at reaching the required specifications (H_2/CO ratio adjustment and CO_2 removal) [4,5], the syngas undergoes the Fischer-Tropsch reaction in order to produce synthetic liquid fuel [6–8]. However, synthesis gas also contains various impurities that must be removed in order to prevent Fischer-Tropsch catalyst poisoning [9–13].

Integrated Gasification Combined Cycles (IGCC) power generation processes also constitutes more efficient and cleaner alternative technology for future energy production [14–16]. As for XTL based Fischer-Tropsch technology, this technology is also based on a first step of feed gasification into a synthesis gas. In IGCC power plants, the syngas is burnt into a gas turbine to produce electrical energy. Synthesis gas impurities such as H_2S, COS and HCN, mixed to H_2, are responsible for the corrosion of the industrial units [17], especially the combustion turbine blades used in IGCC processes.

Among the impurities present in synthesis gases, significant amounts of sulfur and nitrogen compounds are expected whatever the kind of feedstock (fossil or biomass), which are known to be severe poisons for Fischer-Tropsch catalysts [9,10,12,18], and responsible for the corrosion of industrial equipments [17].

Sulfur compounds should be present in the synthesis gas as H_2S and COS, also depending on the gasification process operating conditions [3,11]. The presence of organic species such as mercaptans and thiophenic compounds in synthesis gases obtained from coal gasification is also reported [3]. It however may occur for gasification processes operating at low temperature (fixed or fluidized bed). In gasification processes operating at temperature higher than 1400 °C such as entrained flow reactor, sulfur is only present in the synthesis gas as H_2S and COS, and no organic sulfur compounds should be found downstream according to thermodynamic calculations. Biomass feedstocks generally exhibit a much lower sulfur content than fossil feedstocks (coal, petcoke) [3,11,19,20]. Syngas H_2S and COS contents may thus vary from hundreds to thousands of mol ppm as a function of the feedstock.

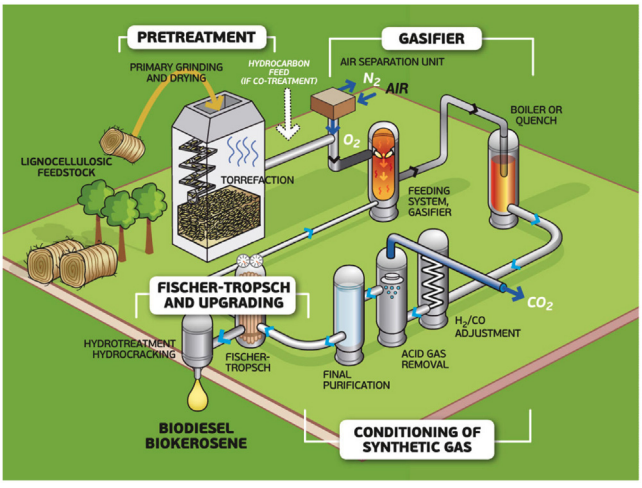

Fig. 1. Schematic representation of the second-generation biofuels production chain from B-XTL thermochemical routes. (source IFPEN).

Nitrogen species present in the feedstocks are converted into HCN and NH_3 in the gasification process. According to literature, the NH_3/HCN ratio depends on many parameters [21–24], such as the nature of feedstocks (that may contain nitrogen compounds with different speciation), operating conditions of the gasification process such as pressure and temperature, gasification process technology (fixed bed, fluidized bed, entrained flow reactor). Nitrogen feedstock contents may vary from 0.1 to 3.3 wt.% [11,25–27], which affect accordingly the resulting nitrogen syngas contents after the gasification step [28]. In the gasification process, HCN formation is predominant from aromatic nitrogen compounds found in fossil feedstocks, whereas combustion of aminoacids and other nitrogen species usually present in biomass predominantly leads to the formation of NH_3 [3,11,22]. Syngas HCN contents may vary from a few mol. ppm to hundreds of mol ppm, and NH_3 contents from a few mol ppm to 14000 mol ppm [3,11]. Other nitrogen compounds might also be present in synthesis gases such as isocyanic acid HNCO, and nitrogen oxides NO_x, also depending on the gasification operating conditions and technology [3,11].

Among existing purification technologies for COS and HCN removal [13,29,30], catalytic processes attract a great deal of interest. Indeed, both COS and HCN impurities can undergo hydrolysis reactions that are thermodynamically highly favored at low temperature. COS and HCN hydrolysis reactions can respectively be written as follows:

$$COS + H_2O \Leftrightarrow CO_2 + H_2S \quad \Delta H = -34,3\,kJ\,mol^{-1} at T = 473\,K$$

$$HCN + H_2O \Leftrightarrow CO + NH_3 \quad \Delta H = -50,7\,kJ\,mol^{-1} at T = 473\,K$$

Catalysts are however required to improve both reactions kinetics. Regarding COS hydrolysis, most studied catalysts in the literature are metal oxides such as TiO_2, Al_2O_3, ZnO and ZrO_2 [13,31–33]. Especially, catalyst activity seems to be related to catalyst surface basicity [34,35]. Alumina and TiO_2 supported catalysts, such as those used as catalysts in Claus processes, are also used for the COS conversion into H_2S. Considering the activation energy, gamma alumina materials might be more active than TiO_2 materials [34,36], and should thus favor COS hydrolysis from lower temperature ($T < 200\,°C$). However, experimental observations evidence water inhibition on gamma alumina materials, occurring through a competitive adsorption on catalyst surfaces which results in a reduction of catalytic activity. As low water contents usually result in an increase of COS conversion, water inhibition effect is reported to occur above a certain H_2O partial pressure, which also depends on COS partial pressure and temperature [33,37,38]. These effects have also been observed on other catalysts such as titania materials. For example, this has been reported in a comparative study on commercial catalysts based on alumina (Kaiser-201, Kaiser Aluminum and Chemicals) and titania (CRS 31, Axens) [36]. Alumina materials, which exhibit relatively high hydrophilic properties, seem to be more affected by catalytic inhibition by water than TiO_2 based materials. Therefore, under operating conditions close to industrial conditions, TiO_2 based catalysts seem to be more active than alumina catalysts. Temperature increase results in a diminution of catalytic inhibition to water, as this favors both kinetic rate

increase and water desorption. More generally, catalytic inhibition is attributed to competitive adsorption with COS, that may hinder its conversion [33,37]. Such phenomena are also very likely to occur with reaction products (CO_2 and H_2S) and other gas compounds that might be adsorbed on catalyst surface [39].

In synthesis gas applications, concomitant COS and HCN removal through hydrolysis process is possible, as catalysts for HCN hydrolysis are reported to be very similar to those used for COS hydrolysis [31]. However, once again a competition between each hydrolysis reaction is likely to occur, through competitive adsorption of reactive species and reaction products on catalysts surface. For each of these reactions, no reaction modeling taking into account any competitive adsorptions has been so far proposed in the literature, while extensive competitive adsorptions phenomena were proven to occur according to experimental data from literature [31,33]. Some kinetics modeling attempts were carried out using an Eley-Rideal model for single COS hydrolysis reaction, assuming COS hydrolysis through interaction of gaseous COS with adsorbed H_2O [36,37]. In the latter, COS conversion through an intermediate adsorbed specie was not considered, in spite of evidences reported for the formation of intermediate surface hydrogeno-thiocarbonate specie [34,39,40].

In this article, we propose COS and HCN hydrolysis reactions modeling, considering for each reaction competitive adsorptions that may result from both reactants and products adsorption, as evidenced in the literature. The model will consider Langmuir-Hinshelwood mechanisms for each reaction, consistent with reported experimental observations [31,33], but never applied for kinetics interpretation and modeling. Both Langmuir-Hinshelwood rate laws proposed for COS and HCN hydrolysis reactions will also consider competitive adsorptions resulting from the simultaneity of both reactions. This kinetic model will be implemented in a complete gas-solid reactor model taking into account all transfer and transport limitations in order to predict industrial performances. Adsorptions of all the reactive species proven to affect reactions kinetics have been taken into account, *i.e.* COS, H_2O, CO_2, H_2S, HCN, NH_3.

In this research, kinetic measurements for COS and HCN hydrolysis have been performed using an industrial TiO_2 based catalyst. Experiments were carried out under controlled conditions using lab scale fixed bed reactors.

2. Material and methods

Kinetic measurements were performed using a batch of an industrial TiO_2 based catalyst, on both uncrushed and crushed catalysts. Uncrushed catalyst is composed of extruded particles with 3 mm diameter. Crushed catalyst particles were obtained after 0,5–1 mm sieving (mean particle size 0.75 mm).

Experiments were carried out under controlled conditions using lab scale fixed bed reactors. A schematic representation of the experimental set-up is reported in Fig. 2. This equipment can be divided in three sections, as represented in Fig. 2:

1. A feed preparation zone where the different gas are mixed to build the feed gas. H_2, CO, CO_2, COS, H_2S, HCN, NH_3 are supplied from gas tanks with specific gas compositions provided by Air Liquide to obtain final gas compositions required for the experiments. Gaseous water is added by evaporation of liquid water dosed by means of a liquid mass flow controller to reach the desired water content.
2. A reaction zone, which basically consists in a cylindrical fixed bed reactor filled with the COS hydrolysis catalyst and heated at the desired temperature.
3. An analytic set-up to analyze and quantify the reactions products through on line mass spectrometry gas analyzer. COS and HCN gas contents upstream and downstream the hydrolysis reaction zone are measured to determine COS and HCN conversion rates as a function of the operating conditions.

Table 1
Reactors dimensions and filling.

	Reactor #1	Reactor #2
Ø	2 cm	4 cm
h	7 cm	16 cm
V	22 mL	201 mL
Catalyst shaping	uncrushed	uncrushed
Catalyst weight	21 g	184 g

Various reactor sizes were used, whose dimensions are reported in Table 1. Solid holdup ε_s (=$1-\varepsilon_b$, with ε_b bed porosity) was measured from loading density d_l and grain density d_g (from Hg porosimetry measurements). Solid holdup values ε_s (=d_l/d_g) were comprised between 0.61 and 0.63. A value of 0.6 is usually typical for fixed bed dense loading. Therefore, channeling was not expected to occur.

3. Theory and calculations

3.1. Hydrolysis reactions kinetics and thermodynamics

A reaction model has been developed, based on a kinetic model validated with experiments obtained in a lab scale fixed bed reactor. First of all, the lab scale reactor is described taking into account all the limitations (external mass transfer and intra particle diffusion) in order to catch the so-called intrinsic kinetic parameters for COS and HCN hydrolysis reactions. Then, the following kinetic model has been implemented in a complete reactor model taking into account all the potential limitations.

As mentioned previously, COS and HCN can react with water according to the following reactions:

$$COS + H_2O \Leftrightarrow CO_2 + H_2S \quad (1)$$

$$HCN + H_2O \Leftrightarrow CO + NH_3 \quad (2)$$

Both reactions are reversible. Thermodynamic equilibrium constants depend on the temperature as shown in Eq. (1′). Table 2 gives the corresponding thermodynamic parameters for the equilibrium constants.

$$\ln\left(K_{eq,i}\right) = \frac{\alpha_i}{T_{(K)}} + \beta_i \quad (1')$$

with i the reaction number ((1) or (2)).

For both reactions, a Langmuir-Hinshelwood reaction mechanism was considered to account for potential co-adsorption of gaseous species on catalyst surface active sites. Kinetic rate expressions for Reactions (1) and (2) are given respectively by Eqs. (2′) and (3′):

$$r_{1_{(mol/s/kg\,cat)}} = k_1 \cdot e^{-\frac{E_1}{RT}} \cdot \frac{\left(P_{COS} \cdot P_{H_2O} - \frac{P_{H_2S} \cdot P_{CO_2}}{K_{eq,1}}\right)}{\left(1 + \sum_i b_i e^{-\frac{\Delta H_i}{RT}} P_i\right)^2} \quad (2')$$

$$r_{2_{(mol/s/kg\,cat)}} = k_2 \cdot e^{-\frac{E_2}{RT}} \cdot \frac{\left(P_{HCN} \cdot P_{H_2O} - \frac{P_{NH_3} \cdot P_{CO}}{K_{eq,2}}\right)}{\left(1 + \sum_i b_i e^{-\frac{\Delta H_i}{RT}} P_i\right)^2} \quad (3')$$

where i stands for each i gaseous compound.

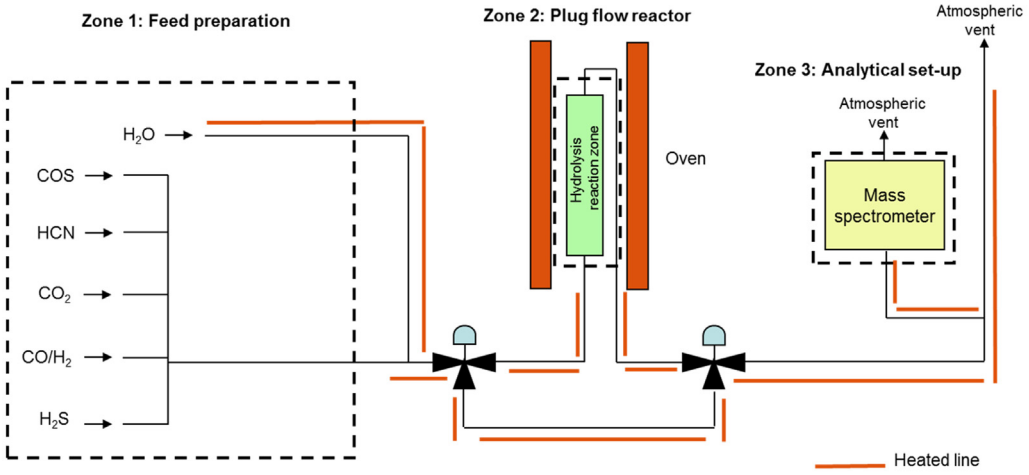

Fig. 2. Schematic representation of the experimental set-up used for kinetic measurements.

Table 2
HCN and COS hydrolysis reactions equilibrium constants.

	α_i	β_i	References
Reaction 1	3796.1	−0.5053	From IFPEN thermodynamic database
Reaction 2	6208.4	−0.5799	Fact sage data http://www.crct.polymtl.ca/fact/

Kinetic parameters for both reactions were estimated from lab scale experiments.

3.2. Reactor modeling

The lab scale fixed bed reactor device has been modeled to study COS and HCN hydrolysis reactions kinetics. A reactor model was developed considering a two-phase (gas-solid) fixed bed system operating under isothermal conditions, due to the low amount of reactants encountered. Indeed, heat transfers have been neglected, as COS and HCN gas contents remain very low, both for the lab scale experiments performed and most industrial cases («1 vol.%). Isothermal conditions assumption was also validated through experiments with temperature measurements conducted with thermocouples located above, inside, and below the catalyst bed. No significant temperature variation was evidenced.

Different catalyst shapes can be used, cylinders or spheres, respectively accounting for experiments using uncrushed or crushed catalyst particles.

Transient material balances are written for each compound at different scales: in the gas flow, in the external mass transfer film around the catalyst particle, and inside the catalyst porous network. However, in this study the model is used to simulate steady-state conditions. The transient description is needed to study some industrial transient procedures such as process startup, runaway, etc., which are not treated in the present work. For the gas flow, a dispersed plug flow model was used in order to take into account potential back-mixing effect. Following Eq. (4′) gives the corresponding transient gas material balance:

$$\varepsilon_g \cdot \frac{\partial C_i^g}{\partial t} = D_{ax}^g \cdot \frac{\partial}{\partial z}\left(\varepsilon_g \cdot \frac{\partial C_i^g}{\partial z}\right) - \frac{\partial\left(v_{sg} \cdot C_i^g\right)}{\partial z} - k_{gs} \cdot \frac{\varepsilon_s}{L_c} \cdot \left(C_i^g - C_i^s\right) \quad (4')$$

Gas axial dispersion coefficient was estimated using the Gunn correlation [41] (Eq. (5′)).

$$D_{ax}^g = \frac{v_{sg}/\varepsilon_g \cdot d_p}{\mathrm{Pe}_a} \quad (5')$$

with $\frac{1}{\mathrm{Pe}_a} = X \cdot (1-\phi)^2 + X^2 \cdot \phi \cdot (1-\phi)^3 \cdot \left[e^{\left(-\frac{1}{X \cdot \phi \cdot (1-\phi)}\right)} - 1\right] + \frac{\varepsilon_g}{\tau_p \cdot Re \cdot Sc}$

and $X = \frac{Re \cdot Sc}{21.13 \cdot \varepsilon_g}$, $Re = \frac{\rho_g \cdot v_{sg} \cdot d_p}{\mu_g}$, $Sc = \frac{\mu_g}{\rho_g \cdot D_m}$

$$\phi = 0.17 + 0.33 \cdot e^{-\frac{24}{Re}}, \quad \tau_p = 1.4 \quad for\ sphere$$

$$\phi = 0.17 + 0.29 \cdot e^{-\frac{24}{Re}} \quad \tau_p = 1.93 \quad for\ cylinder$$

The material balance in the external film is given by Eq. (6′):

$$\delta \cdot \frac{\partial C_i^s}{\partial t} = k_{gs} \cdot \left(C_i^g - C_i^s\right) - D_{eff,i} \cdot \frac{\partial C_i^p}{\partial r}\Big|_{r=R_p} \quad (6')$$

with $\delta = \frac{D_m}{k_{gs}}$ (film thickness) and $L_c = \frac{V_p}{A_p}$(characteristic length of the catalyst).

The mass transfer coefficient $k_{gs,i}$ for each specie i is given by the Yoshida correlation [42], which takes into account the gas flow pattern around the particle (Eq. (7′)).

$$\mathrm{Sh} = 0.983 \cdot Re^{0.59} \cdot \mathrm{Sc}^{1/3} \quad if\ Re > 190$$
$$\mathrm{Sh} = 1.66 \cdot Re^{0.49} \cdot \mathrm{Sc}^{1/3} \quad if\ Re < 190 \quad (7')$$

with $\mathrm{Sh} = \frac{k_{gs,i} \cdot d_p}{D_{m,i}}$, $Re = \frac{\rho_g \cdot v_{sg} \cdot d_p}{\mu_g}$, $\mathrm{Sc} = \frac{\mu_g}{\rho_g \cdot D_{m,i}}$.

Gas material balances should respect the equation of state $\sum_i C_i^g = \frac{P_t}{R.T}$ (ideal gas law assumption). Then, after summing all the gas equations and introducing the equation of state, the corre-

sponding equation for the gas velocity is obtained (Eq. (8′)):

$$\frac{\partial\left(v_{sg}\cdot P_t\right)}{\partial z} = D_{ax}^{g}\cdot\frac{\partial}{\partial z}\left(\varepsilon_g\cdot\frac{\partial P_t}{\partial z}\right) - R\cdot T\cdot\sum_i k_{gs,i}\cdot \frac{\varepsilon_s}{L_c}\cdot\left(C_i^g - C_i^s\right) \quad (8')$$

Particle material balances (Eqs. (9′) and (10′)) are written for two particle shapes, cylinders and spheres, respectively accounting for uncrushed and crushed catalyst particles.

Spherical particle modeling:

$$\varepsilon_p.\frac{\partial C_i^p}{\partial t} = \frac{D_{eff,i}}{r^2}.\frac{\partial\left(r^2.\frac{\partial C_i^p}{\partial r}\right)}{\partial r} + \sum_j \mu_{i,j}.r_j.\rho_s \quad (9')$$

Cylindrical particle modeling:

$$\varepsilon_p.\frac{\partial C_i^p}{\partial t} = \frac{D_{eff,i}}{r}.\frac{\partial}{\partial r}\left(r.\frac{\partial C_i^p}{\partial r}\right) + \sum_j \mu_{ij}.r_j.\rho_s \quad (10')$$

with ε_p particle porosity.

The effective diffusion coefficient is a function of the molecular diffusion coefficient of each compound, and of catalyst porosity and tortuosity (Eq. (11′)):

$$D_{eff,i} = \frac{D_{m,i}\cdot\varepsilon_p}{\tau_p} \quad (11')$$

where τ_p stands for catalyst tortuosity ($2 < \tau_p < 5$), and ε_p catalyst porosity. Following default catalyst tortuosity and porosity values $\tau_p = 2.5$ and $\varepsilon_p = 0.5$ were considered for the modeling (arbitrary set values).

Effect of pressure and temperature on the molecular diffusion coefficient has been taken into account. Calculations of gas molecular diffusion have been carried out from Eq. (12′), as given by *Fuller* et al. [43]:

$$D_{iB} = \frac{1.43\cdot 10^{-3}\cdot T^{1.75}}{P_t\cdot M_{iB}^{1/2}\cdot\left[\left(\Sigma_v\right)_i^{1/3} + \left(\Sigma_v\right)_B^{1/3}\right]^2} \quad with \quad M_{iB} = \frac{2}{\frac{1}{M_i}+\frac{1}{M_B}} \quad (12')$$

With D_{iB} binary diffusion coefficient of compound i in a matrix B (gaseous diluent). Binary diffusion coefficients were estimated considering CH_4 as gaseous diluent (averaged physical properties compared to H_2-CO-CO_2-H_2O mixtures used for the experiments).

Reactor pressure drop is calculated using the Ergun relation [44] (Eq. (13′)) or the Handley relation [45] (Eq. (14′)) according to the gas flow regime.

$$\frac{dP}{dz} = \frac{150}{d_p^2}.\frac{\varepsilon_s^2}{(1-\varepsilon_s)^3}.\mu_g.v_{sg} + \frac{1.75}{d_p}.\frac{\varepsilon_s}{(1-\varepsilon_s)^3}.\rho_g.v_{sg}^2 \quad 0 < \mathrm{Re}/\varepsilon_s < 1000 \quad (13')$$

$$\frac{dP}{dz} = \frac{368}{d_p^2}.\frac{\varepsilon_s^2}{(1-\varepsilon_s)^3}.\mu_g.v_{sg} + \frac{1.24}{d_p}.\frac{\varepsilon_s}{(1-\varepsilon_s)^3}.\rho_g.v_{sg}^2 \quad 1000 < \mathrm{Re}/\varepsilon_s < 5000 \quad (14')$$

3.3. Numerical resolution

A spatial discretization of the partial derivative equations was performed using an upwind finite differences scheme for the convection terms, and a centered finite differences scheme for the diffusion or dispersion terms. For time integration, the LSODE solver was used based on a predictor-corrector algorithm [46]. An excel interface coupled with Matlab (for 3D visualization) was developed.

Table 3
Operating conditions ranges (T, P, gas composition).

	Laboratory operating conditions ranges
T	60, 100, 120, 160, 180, 190, 200, 220, 240, 280 °C
P	1, 5, 7, 10, 20 bar
GHSV	300–23000 h^{-1}
H_2	25–57 vol.%
CO	22–55 vol.%
CO_2	1.3, 5, 9.5 vol.%
H_2O	0.5, 2, 4, 8, 10, 18 vol.%
COS	0, 200, 250, 500, 1000, 2000 vol. ppm
H_2S	0, 2000, 10000, 20000 vol. ppm
HCN	0, 250, 350, 500, 1000 vol. ppm
NH_3	0, 500, 7000 vol. ppm

3.4. Model parameters optimization

Adsorption and kinetic parameters have been estimated using a Levenberg-Marquardt optimizing method [47]. This approach is based on a controlled Newton-Gauss numerical method. A statistical analysis of the optimized parameters is performed and a corresponding confidence interval of 95% is given for each of them. It is a way to evaluate the statistical significance of a parameter, and to verify if the results from the model and the experimental data set are sensitive to it. The correlation matrix coming from this statistical analysis allows to help to choose the right experimental data subset to discriminate effects of correlated parameters. A part of the experimental data set is used for parameter optimization (experiments with COS or HCN conversion < 80%) and another part is used for model validation.

4. Results and discussion

4.1. Experimental data

COS and HCN hydrolysis reactions over an industrial TiO_2 based catalyst in fixed bed reactor configuration have been studied. The experiments performed are aimed at validating Langmuir-Hinshelwood type rate laws and determining the sensitivity of reactions kinetics to operating parameters, namely reactants gas contents, temperature, and residence time. Residence times have been set to reach partial COS and HCN conversions (lower than 80% in most cases) to be able to monitor conversion variations as a function of other operating parameters (gas composition and temperature). This allowed to identify critical operating parameters, and especially gas compounds that affect reactions kinetics.

COS and HCN conversion rates achieved as a function of operating parameters for each experiments are then used for the validation of kinetic rates laws expected (Langmuir-Hinshelwood), and kinetic parameters determination through the model developed.

Influence of the following parameters on COS and HCN hydrolysis extent has been explored: reactants partial pressures (*i.e.* COS, H_2O, H_2S, CO_2, HCN, NH_3), operating temperature, total pressure, residence time (through variation of the gas hourly space velocity (GHSV)). All the experiments have been performed in a synthesis gas matrix (in a H_2 – CO – CO_2 mixture). Operating temperatures, pressure ranges, and gas composition explored are summarized in Table 3. Finally, 144 experiments have been performed, with 92 experiments for which partial COS and HCN conversion have been reached (lower than 80%). In the following, kinetic conversion rates are expressed as a function of normalized residence time values, defined as the ratio of residence time τ and a constant reference time value τ_0.

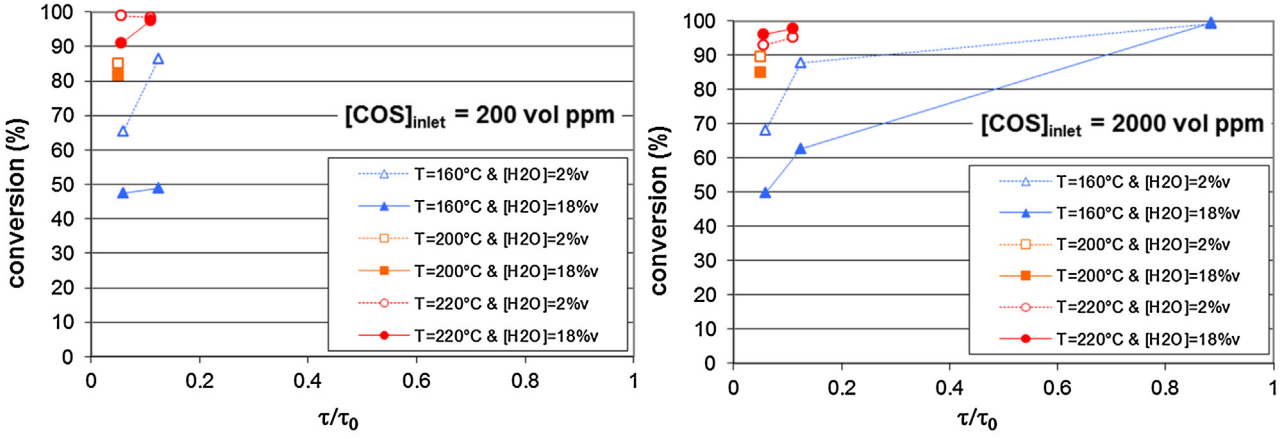

Fig. 3. COS conversion rate as a function of temperature, water content and normalized residence time, for various COS inlet gas contents.

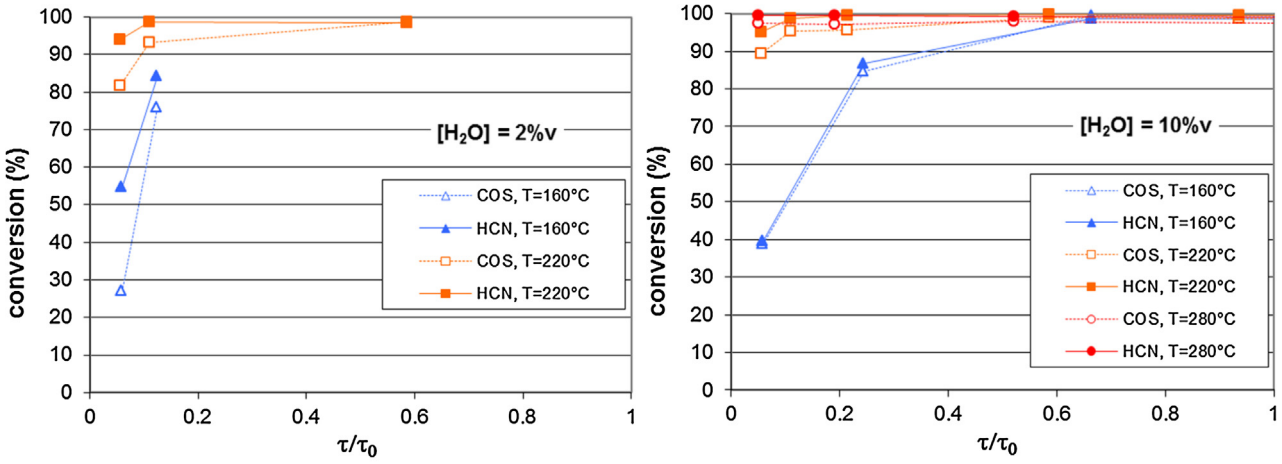

Fig. 4. COS and HCN conversion rates as a function of temperature and normalized residence time, for various H_2O gas content, and for COS inlet gas content of 2000 vol. ppm and HCN inlet gas content of 500 vol. ppm.

4.1.1. Effect of temperature

For each COS and HCN hydrolysis reaction, effect of temperature on conversion rate was explored. Fig. 3 shows some of the results obtained for the hydrolysis of COS alone (no HCN nor NH_3). It shows COS conversion rate, as a function of temperature and residence time, for various initial COS and water gas contents. As expected, higher conversion rates are achieved with temperature increase. High conversion rates (>98%) are obtained for temperatures above 220 °C and/or long residence times (normalized residence times values $\tau / \tau_0 > 0.5$). Lower conversion rates are obtained for normalized residence times values τ / τ_0 comprised between 0.05 and 0.25. These experiments achieved with low residence times can be used to explore COS hydrolysis reaction kinetics sensitivity to other operating parameters, by monitoring conversion rates variations.

Similar experiments were carried out on gas containing HCN and no COS nor H_2S to evaluate the effect of temperature upon HCN hydrolysis over the TiO_2 based catalyst (results not shown). Concomitant COS and HCN hydrolysis experiments were also performed. Fig. 4 shows some of the results obtained in the latter case.

4.1.2. Effect of H_2O gas content

Although H_2O is a reactant and allows COS and HCN hydrolysis, water molecules may compete with other reactants or reaction products over adsorption on catalyst surface. Therefore, some experiments have been carried out to investigate possible inhibition of catalytic activity toward COS and HCN hydrolysis with increasing gas water content. Effect of temperature is also considered, as it may affect reactants adsorption. These experiments have been achieved for the study of separate COS hydrolysis (as shown in Fig. 3), HCN hydrolysis (results not shown), and concomitant COS and HCN hydrolysis (as shown in Fig. 4). Some of the results obtained are represented as a function of the initial H_2O gas content in Fig. 5. A decrease of both COS and HCN conversion rates is observed at 160 °C with increasing H_2O gas content. At 220 °C, increase of H_2O content does not affect conversion rates; one should however notice that due to the high conversion values measured at 220 °C, the operating condition ranges explored for this latter set of experiments do not allow to highlight the influence of water on reaction kinetics (lower residence times would be necessary here). Other consistent data (not shown) were acquired at intermediate temperatures (180 °C and 200 °C), and below 160 °C (60 °C, 100 °C, 120 °C). These experiments clearly evidence an inhibition of catalytic activity below 180 °C for the operating conditions ranges explored.

4.1.3. Effect of H_2S and NH_3

COS and HCN hydrolysis reaction products might also act as catalytic reaction inhibitors, through competitive adsorption on catalyst surface. The effects of H_2S and NH_3 on COS and HCN hydrolysis reactions have been investigated. Fig. 6 shows COS and HCN conversion rates as a function of H_2S initial gas content. No effect is

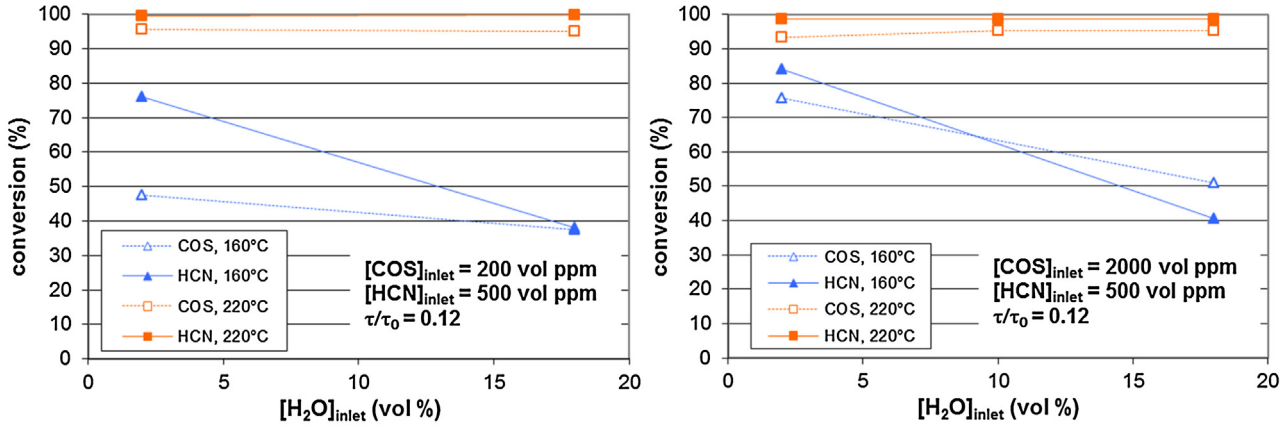

Fig. 5. COS and HCN conversion rates as a function of gas water content, for various operating temperatures, and inlet COS gas content. Residence time set is the same for each experimental point.

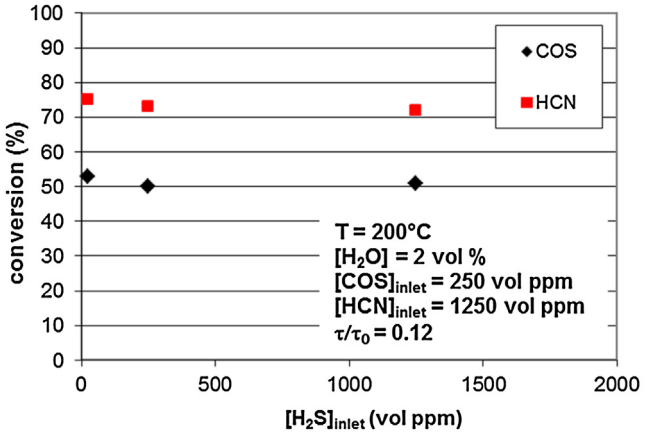

Fig. 6. COS and HCN conversion rates as a function of H_2S inlet gas content. Residence time set is the same for each experimental point.

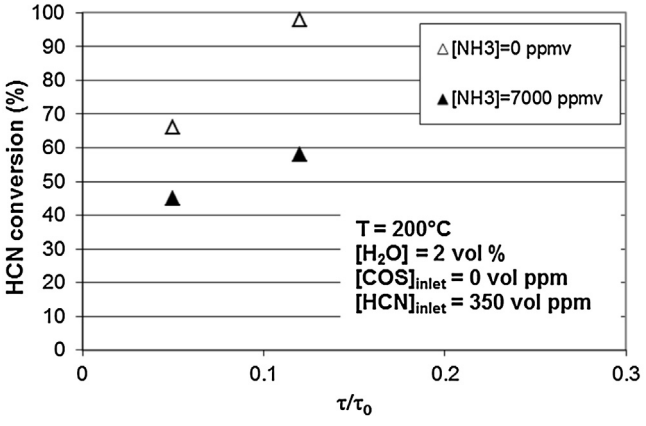

Fig. 7. HCN conversion rate as a function of NH_3 inlet gas content and normalized residence time.

evidenced on COS and HCN conversion kinetics. As a consequence, H_2S does not seem to compete toward HCN and COS adsorption on TiO_2 catalyst.

However, presence of NH_3 in the gas significantly affects HCN conversion. Fig. 7 shows some of the results obtained in the case of HCN hydrolysis. NH_3 has therefore to be taken into account for reaction modeling.

When TiO_2 surfaces are activated with temperature (and without water), NH_3 is known to strongly interact with TiO_2 surface Lewis acid-sites [48–50]. However, the experiments presented in the paper were all conducted in the presence of water, and under temperatures where TiO_2 surfaces are kept hydrated (≤220 °C for most of the experiments allowing COS and HCN conversions lower than 80%). In these conditions, NH_3 is more likely to interact through H-bonding with titania OH surface groups [48,49]. Some stronger interactions might also occur in these conditions, but this was not investigated in the field of this study.

4.1.4. Simultaneous HCN and COS hydrolysis reactions

As also shown previously, concomitant COS and HCN hydrolysis experiments were carried out to explore how each reaction may affect each other. As previously discussed, according to literature [31–34,39], each COS and HCN hydrolysis reactions are expected to occur through adsorption of COS and HCN reactants and reaction products upon catalyst surface. As it was shown from previous experiments discussed, high H_2O gas contents and NH_3 (for the operating ranges explored) were shown to affect kinetics, more likely through a competitive adsorption upon HCN and COS adsorption sites. This resulted in an inhibition of catalytic activity. No effect of H_2S was evidenced in the operating conditions ranges explored (no competitive adsorption upon HCN and COS adsorption sites). Simultaneous COS and HCN hydrolysis experiments are therefore aimed at investigating whether simultaneous presence of HCN and COS species may affect each other upon their conversion kinetics. A full range of experiments has been carried out, showing significantly lower conversion rates for simultaneous COS and HCN hydrolysis, compared to conversion rates measured with COS or HCN alone in the same conditions. Fig. 8 shows some of results obtained for experiments with COS alone compared to same experiments with HCN added. These results clearly evidence a detrimental effect of the presence of HCN upon COS conversion. Catalytic inhibition effect could therefore result from the presence of HCN, and also from the presence of NH_3 formed through HCN hydrolysis. Similar results are obtained for HCN conversion, that evidence HCN conversion inhibition in the presence of COS (results not shown).

4.2. Hydrolysis reactions modeling

The experimental data (COS and HCN conversion rates as a function of operating conditions) were used to fit kinetic and adsorption constants of Langmuir-Hinshelwood kinetic rate laws for both COS and HCN hydrolysis reactions catalyzed by the industrial TiO_2 based

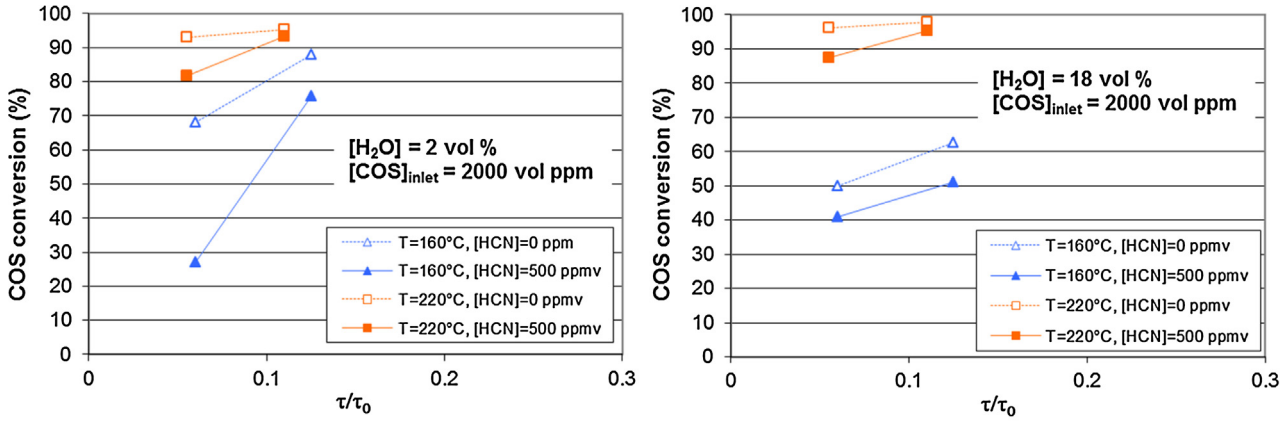

Fig. 8. COS conversion rate as a function of HCN gas content and normalized residence time, for COS inlet gas content of 2000 vol. ppm, and for various operating temperatures and H_2O gas contents.

Table 4
Optimized parameters and statistical analysis.

	Kinetic parameters				*Statistic test*
	Estimated values	Standard deviation	Lower limit	Upper limit	*t*-value
k_1/k_1°	1.00	0.98	−1.07	2.85	0.9
k_2/k_1°	2.41	5.11	−7.63	12.82	0.5
E_1/E_1°	1.00	0.18	0.63	1.37	5.4
E_2/E_1°	1.11	0.33	0.44	1.78	3.3
b_{COS} (Pa^{-1})	4.49E-07	2.28E-06	−4.10E-06	5.00E-06	0.02
b_{HCN} (Pa^{-1})	1.67E-03	1.39E-03	−1.11E-03	4.46E-03	1.2
b_{NH3} (Pa^{-1})	1.07E-11	3.24E-11	−5.42E-11	7.56E-11	0.3
b_{H2O} (Pa^{-1})	7.44E-07	6.19E-07	−4.93E-07	1.98E+06	1.2
ΔH_{COS} ($J\,mol^{-1}$)	−7054	35000	−77000	62900	−0.2
ΔH_{HCN} ($J\,mol^{-1}$)	−10829	3250	−17300	−4340	−3.3
ΔH_{NH3} ($J\,mol^{-1}$)	−75314	11700	−98600	−52000	−6.5
ΔH_{H2O} ($J\,mol^{-1}$)	−21646	2860	−27400	−15900	−7.6

Table 5
Correlation matrix for kinetic and adsorption constants determined from the model optimization. Values are closer to one for parameters strongly correlated (bold values).

	k_1	k_2	E_1	E_2	b_{COS}	b_{HCN}	b_{NH3}	b_{H2O}	ΔH_{COS}	ΔH_{HCN}	ΔH_{NH3}	ΔH_{H2O}
k_1	**1.00**	0.01	**0.98**	0.02	−0.24	−0.03	0.11	−0.39	−0.05	0.00	0.06	−0.42
k_2	0.01	**1.00**	0.04	**0.99**	−0.33	0.47	−0.87	−0.10	−0.34	0.42	−0.83	−0.07
E_1	**0.98**	0.04	**1.00**	0.06	−0.25	−0.03	0.10	−0.45	−0.07	0.05	0.06	−0.44
E_2	0.02	**0.99**	0.06	**1.00**	−0.31	0.45	−0.85	−0.14	−0.33	0.43	−0.81	−0.09
b_{COS}	−0.24	−0.33	−0.25	−0.31	**1.00**	−0.32	0.13	0.06	**0.97**	−0.34	0.16	0.04
b_{HCN}	−0.03	0.47	−0.03	0.45	−0.32	**1.00**	−0.66	−0.02	−0.34	**0.96**	−0.67	−0.02
b_{NH3}	0.11	−0.87	0.10	−0.85	0.13	−0.66	**1.00**	0.06	0.17	−0.59	**0.97**	0.04
b_{H2O}	−0.39	−0.10	−0.45	−0.14	0.06	−0.02	0.06	**1.00**	0.11	−0.11	0.07	**0.98**
ΔH_{COS}	−0.05	−0.34	−0.07	−0.33	**0.97**	−0.34	0.17	0.11	**1.00**	−0.37	0.19	0.08
ΔH_{HCN}	0.00	0.42	0.05	0.43	−0.34	**0.96**	−0.59	−0.11	−0.37	**1.00**	−0.62	−0.07
ΔH_{NH3}	0.06	−0.83	0.06	−0.81	0.16	−0.67	**0.97**	0.07	0.19	−0.62	**1.00**	0.06
ΔH_{H2O}	−0.42	−0.07	−0.44	−0.09	0.04	−0.02	0.04	**0.98**	0.08	−0.07	0.06	**1.00**

catalyst used in this study, according to the procedure described in Section 3.

Kinetic constants k_i, and activation energies E_i for both reactions, as well as adsorption constants b_i and ΔH_i for each gaseous compound were estimated through kinetic model optimization from a first restricted set of experiments. This first set of 46 experiments was chosen from experiments showing most significant sensitivity toward operating parameters (temperature, and gas composition). This was performed in order to facilitate parameters optimization. The whole set of parameters was optimized simultaneously. Table 4 shows the optimized values of the activation energies, adsorption constants and enthalpies with the corresponding confidence intervals and *t*-values. Normalized kinetics constants and activation energies values of both COS and HCN hydrolysis reactions are reported, taking as a reference values obtained for the COS hydrolysis reaction k_1° and E_1°. This allows comparison between values obtained for both COS and HCN hydrolysis reactions.

Only five parameters (activation energies and adsorption enthalpies) are significant according to confidence intervals. The correlation matrix shows that pre-exponential factors b_i are strongly correlated with the corresponding energies ΔH_i (*Cf.* Table 5). This correlation can be explained by the linear trend of exponential terms when the temperature range explored is too narrow. A wider experimental temperature range should be explored to de-correlate adsorption enthalpies from pre-exponential factors. Therefore, it was decided to set constant adsorption enthalpy values, in order to make sensitive the pre-exponential factors.

Table 6 with *t*-values reported from the statistic test shows that most of the pre-exponential factors become significant (*t*-values ≥ 2) when energy values are set constant. This means that the experimental data set is able to sensitize the activities and the

Table 6
Statistical analysis of the parameters with adsorption enthalpy values set constant.

	Kinetic parameters				*Statistic test*
	Estimated values	Standard deviation	Lower limit	Upper limit	*t*-value
k_1/k_1°	1.00	0.33	0.23	1.54	2.7
k_2/k_1°	2.41	0.81	0.97	4.21	3.2
b_{COS} (Pa^{-1})	4.49E-07	2.31E-04	−4.61E-04	4.62E-04	0.002
b_{HCN} (Pa^{-1})	1.67E-03	3.67E-04	9.38E-04	2.41E-03	4.6
b_{NH3} (Pa^{-1})	1.07E-11	5.58E-12	−4.49E-13	2.19E-11	1.9
b_{H2O} (Pa^{-1})	7.44E-07	1.39E-07	4.67E-07	1.02E-06	5.4

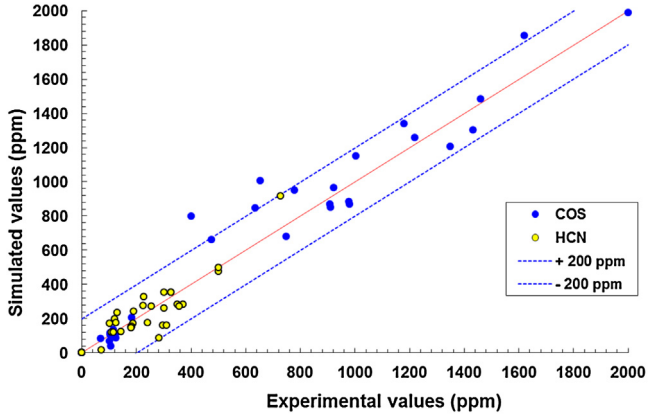

Fig. 9. Parity diagram giving calculated COS and HCN gas content from model optimization as a function of related experimental COS and HCN content after reaction. Results obtained for the first set of 46 experiments used for parameters optimization are represented.

adsorptions of many species. Nevertheless, COS adsorption does not seem to have a significant impact, as *t*-values are close to 0 for COS adsorption parameters, and as $b_{COS} \cdot \exp(-\Delta H_{COS}/RT)$ values can be neglected in comparison to other adsorption terms on the whole temperature range explored. This may result from a lack of information in the experimental data set used for the modeling. Another possibility is that adsorption of these compounds could be neglected as it would not significantly affect reactions kinetics. The latter would be in agreement with previous high temperature COS hydrolysis modeling through Eley-Rideal mechanism performed by *Tong* et al. on other TiO_2 based catalyst [36]. Further experimental investigations should be carried out in order to discriminate between both hypotheses.

Kinetic constants values have been compared to values reported for an Eley-Rideal modeling, and obtained for COS hydrolysis on another TiO_2 based catalyst on temperature range of 270 °C–330 °C [36]. Reported kinetic constants as a function of temperature are in the same order of magnitude (*Cf.* Table 7), even though temperature range explored for both studies and the catalyst used are different. No data were found regarding HCN hydrolysis on similar materials; kinetic constants can be found calculated on other materials (model materials Al_2O_3 and TiO_2) and with other formalism [31].

Adsorption constants values obtained for HCN, NH_3, H_2O are therefore in agreement with a competition model for adsorption of these species towards catalyst active sites. Each specie compete towards adsorption on surface active sites, and may therefore interfere between each other for adsorption. As shown in experimental parts, the presence of NH_3 and H_2O (over a certain amounts for the latter) results in an inhibition of catalytic activity for both COS and HCN reactions.

Furthermore, as the experiments did not show any sensitivity of the presence of H_2S, and of gaseous major compounds (H_2, CO, CO_2) upon hydrolysis reactions kinetics (for operating conditions ranges explored), adsorption constants for these species calculated from model optimization were logically equal to 0. General Langmuir-Hinshelwood kinetic rate laws given in Eq. (2′) and Eq. (3′) for both reactions can therefore be expressed according to the following:

$$r_{1_{(mol/s/kg\,cat)}} = k_1 \cdot e^{-\frac{E_1}{RT}} \cdot \frac{\left(P_{COS} \cdot P_{H_2O} - \frac{P_{H_2S} \cdot P_{CO_2}}{K_{eq,1}}\right)}{\left(1 + b_{HCN} e^{-\frac{\Delta H_{HCN}}{RT}} P_{HCN} + b_{H_2O} e^{-\frac{\Delta H_{H_2O}}{RT}} P_{H_2O} + b_{NH_3} e^{-\frac{\Delta H_{NH_3}}{RT}} P_{NH_3}\right)^2} \quad (15')$$

$$r_{2_{(mol/s/kg\,cat)}} = k_2 \cdot e^{-\frac{E_2}{RT}} \cdot \frac{\left(P_{HCN} \cdot P_{H_2O} - \frac{P_{NH_3} \cdot P_{CO}}{K_{eq,2}}\right)}{\left(1 + b_{HCN} e^{-\frac{\Delta H_{HCN}}{RT}} P_{HCN} + b_{H_2O} e^{-\frac{\Delta H_{H_2O}}{RT}} P_{H_2O} + b_{NH_3} e^{-\frac{\Delta H_{NH_3}}{RT}} P_{NH_3}\right)^2} \quad (16')$$

Parity diagram showing calculated COS and HCN conversions from model optimization as a function of related experimental conversions is represented in Fig. 9. The results obtained for the first set of 46 experiments used for parameters optimization are represented. This shows good agreement between experimental and calculated values.

Parity diagram showing calculated versus experimental conversions for the whole 92 experiments exhibiting partial COS and HCN conversions (<80%) is represented in Fig. 10. Some discrepancies are evidenced, as some simulated values result in an overestimation of COS and HCN remaining contents compared to experimental values. Discrepancies seem to be higher for COS conversion than for HCN. This might be explained by the high amount of CO_2 considered in gas matrix, and as CO_2 was not taken into account for the experimental sensitivity study (as present in high concentration in synthesis gas applications). Indeed, CO_2 may also compete with COS on similar adsorption sites [38,39].

Table 7
Comparison with COS hydrolysis kinetic constant as reported from Tong et al. for an Eley-Rideal modeling of data obtained on other TiO_2 based catalyst [36].

T (°C)	270	300	330
Kinetics constants ratio $\frac{k \cdot K_3}{k_1 \cdot e^{-\frac{E_1}{RT}}}$	3.6	1.9	1.3

With $k.K_3$ the COS hydrolysis kinetic constant from Eley-Rideal model as reported by *Tong* et al. (*Tong et al.* notation), and $k_1.e^{(-E1/RT)}$ the COS hydrolysis kinetic constant from the Langmuir-Hinshelwood model as calculated in the present study.

Table 8
Estimation of transport limitations from Thiele modulus calculations for some representative experimental conditions. Numerical application to the case of COS hydrolysis reaction.

Mean particle diameter:	Lab-scale experiments			
	Uncrushed (cylindrical particle): d_p = 3 mm		Crushed (spherical particle): d_p = 0.75 mm	
T	150 °C	220 °C	150 °C	220 °C
Thiele modulus m_T	1.07	2.64	0.18	0.44

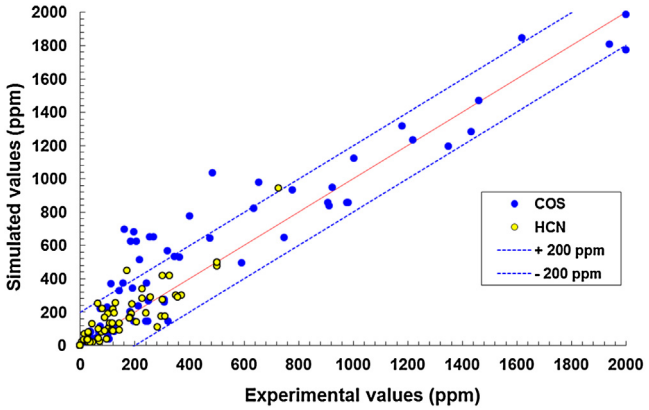

Fig. 10. Parity diagram giving calculated COS and HCN gas content from model optimization as a function of related experimental COS and HCN content after reaction, for the whole 92 experiments (with conversions lower than 80%).

Significant transport limitations are observed at the bed inlet due to the high reaction rates. Low transport limitations are observed at reactor outlet, due to lower COS and HCN gas content resulting from hydrolysis reactions along the reactor. COS and HCN intra particle concentrations profiles at different reactor elevations calculated from the reaction model are represented in Fig. 11.

A data analysis can be performed from Thiele modulus calculations to further estimate the extent of macroporous diffusion limitations evidenced from the modeling. Thiele modulus calculations give an estimation of the limitations encountered, which are function of the relative importance of reaction kinetics towards mass transport [51]. The expression of Thiele modulus derived from *Rajadhyaksha* et al. in the case of Langmuir-Hinshelwood kinetics has been used [52]. Thiele modulus m_T is given by the following relation (Eq. (17′)), as expressed using the article notation in the case of COS hydrolysis reaction:

$$m_T = \frac{1}{1 + b_{COS} \cdot e^{-\frac{\Delta H_{COS}}{RT}} \cdot P_{COS}} \cdot \sqrt{\frac{P_{COS}}{\ln\left(1 + b_{COS} \cdot e^{-\frac{\Delta H_{COS}}{RT}} \cdot P_{COS}\right)}} \cdot L_c \cdot \sqrt{\frac{k_1 \cdot e^{-\frac{E_1}{RT}}}{b_{H_2O} \cdot e^{-\frac{\Delta H_{H2O}}{RT}}} \cdot \frac{1}{D_{COS}}} \qquad (17')$$

with k_1 the kinetic rate constant as calculated from the modeling for the COS hydrolysis reaction (*Cf.* Section 4.2), E_1 activation energy for COS hydrolysis, b_{COS} and ΔH_{COS} respectively the COS adsorption constant and enthalpy, D_{COS} the effective molecular diffusion coefficient of COS (calculated from the Fuller correlation [43], *Cf.* Eqs. (11') and (12′)), L_c the particle characteristic length defined as the ratio of particle volume V_p over particle external surface A_p.

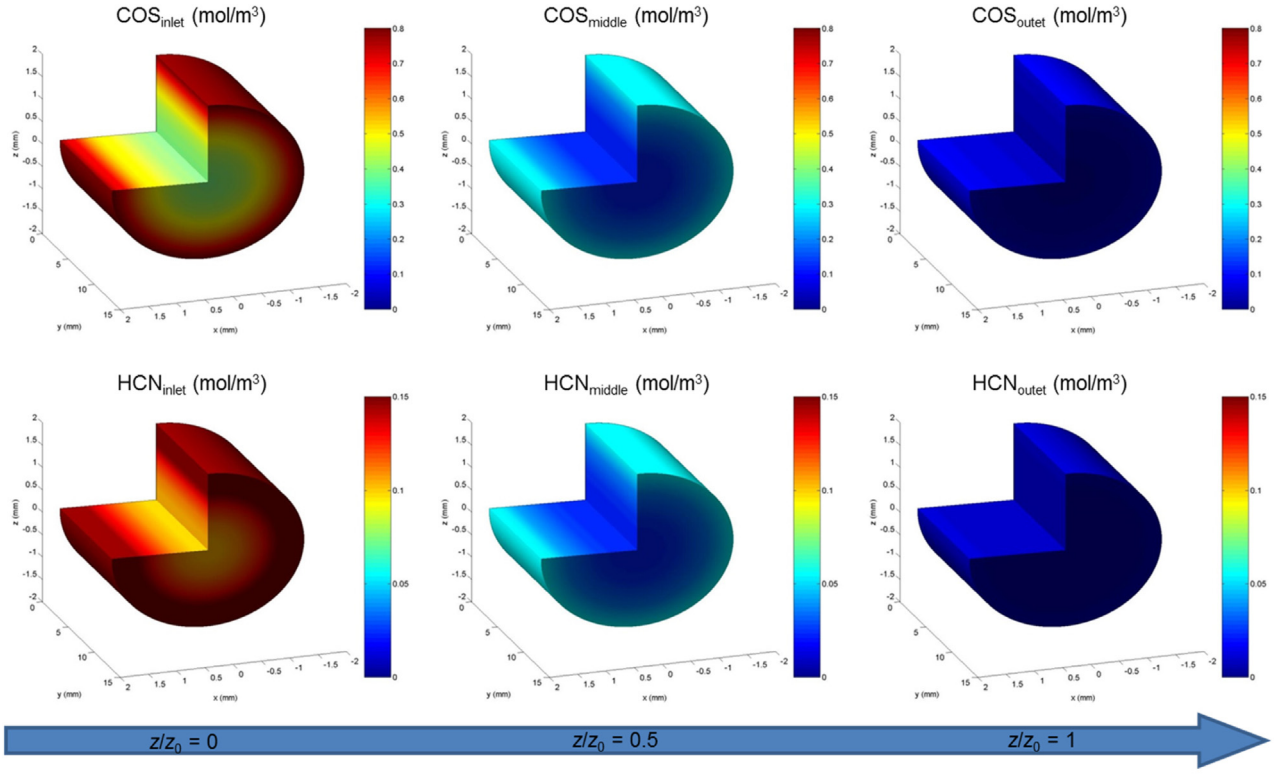

Fig. 11. Example of particle COS and HCN concentration profiles at different axial positions in the reactor (z/z_0).

Thiele modulus calculations for some operating conditions for lab scale experiments as a function of particle size (crushed *vs.* uncrushed particles) are given in Table 8. Thiele modulus values $m_T > 1$ evidence mass transport limitations, whereas kinetics limitations are evidenced for $m_T < 1$. The calculations reported in Table 8 show for uncrushed particles that the higher the temperature, the higher the reaction kinetics along with induced mass transport limitations. Together with kinetics and 3D modeling of reactants and products gradients inside particles (Fig. 11), this shows the occurrence of mass transport limitations inside catalyst porosity, due to significantly high catalyst activity for the COS hydrolysis reaction (high kinetic rate favored with increasing temperature). As a consequence, the extent of mass transport limitations will be also more pronounced with increasing particle size and/or pressure (the latter affecting molecular diffusivity). Same conclusions arise from the data analysis performed for the HCN hydrolysis reaction (not shown).

Interest for other shapes of catalyst particle is therefore clearly evidenced, such as multilobe shapes (*e.g.* trilobe, ...), whose specific outer surface is increased and characteristic diameter decreased. Such shapes would contribute to enhance catalyst efficiency, taking advantage of the high catalytic activity, and lowering the intra particle diffusional limitations resulting from the fast reactions kinetics.

5. Conclusions

COS and HCN hydrolysis reactions over an industrial TiO_2 based catalyst were extensively studied in this work. 144 experiments were carried out, including 92 experiments that allowed to achieve partial conversion rates and showed reaction kinetics sensitivity to operating parameters. Significant crossed influences were evidenced between both COS and HCN hydrolysis reactions. The concomitant occurrence of both reactions showed to detrimentally affect each other upon COS and HCN conversion rates, and therefore upon kinetic rates. This was explained through a competitive adsorption of HCN and COS upon catalyst surface active sites. Inhibition of catalytic activity by the presence of NH_3 and H_2O (over a certain amount for the latter) was also evidenced. For the operating conditions ranges explored, H_2S and CO_2 had no sensitive impact on the kinetics of the COS and HCN hydrolysis reactions. However the moderate impact of CO_2 upon COS and HCN conversion rates might be explained by the large CO_2 excess compared to COS and HCN levels. High amounts of CO_2 were indeed considered for lab scale tests, as typical synthesis gas matrices were used. However, one should also expect detrimental effect of the presence of CO_2 due to competitive adsorption towards catalytic active sites. For higher conversion rates, the presence of H_2S and CO_2 may also decrease the conversion performances due to thermodynamic equilibrium limitations.

A full reaction model has been developed considering hydrodynamic, external mass transfer and intra particle diffusion limitations, and Langmuir-Hinshelwood reaction mechanisms for both COS and HCN hydrolysis reactions. Langmuir-Hinshelwood kinetic rate laws were considered to account for the detrimental effect of gaseous species upon COS and HCN conversion kinetic rates, through competitive adsorption upon catalyst active sites of COS, HCN, H_2O, and NH_3. Collected kinetic data as a function of reactor size, gas residence time, temperature and reactants partial pressures were used to validate and fit kinetic and adsorption constants. Good agreement was achieved between experimental and calculated COS and HCN conversion rates from the model developed. This allowed to validate the Langmuir-Hinshelwood kinetic rate laws. Additional experimental work has to be carried out to evaluate more accurately the contribution of COS and NH_3 adsorption. Moreover, a larger temperature range should be explored in order to de-correlate pre-exponential factors from corresponding adsorption enthalpies. Catalyst acid-base surface characterizations should also allow a better determination and understanding of the nature of the surface sites involved in each step of the reactions, and of the relative reactivity of surface sites toward reactants and products adsorption.

Langmuir-Hinshelwood kinetic rate laws included in the plug flow reactor model developed can be used as a powerful modeling tool for a better understanding of physical-chemical phenomena involved in both COS and HCN hydrolysis reactions upon an industrial TiO_2 based catalyst. This coupled hydrodynamic-reaction model also constitutes a complete industrial reactor model taking into account all the potential limitations, and can be used as a powerful predicting tool for industrial process design, *i.e.* fully usable for industrial process scale-up and optimization purposes.

Intra particle diffusional limitations were evidenced, resulting from fast reactions kinetics. Interest for other shapes of catalyst is therefore clearly evidenced, such as multilobe shapes (*e.g.* trilobe, ...), which would contribute to enhance catalyst efficiency, taking advantage of the high catalytic activity, and lowering the intra particle diffusional limitations resulting from the fast reactions kinetics.

Acknowledgment

The authors thank Jean-Pierre Reyt (IFPEN) for technical help on catalytic apparatus.

References

[1] A. Demirbas, Prog. Energy Combust. Sci. 33 (2007) 1–18.
[2] D. Ballerini, Biofuels – Meeting the Energy and Environmental Challenges of the Transportation Sector, Editions Technip, 2012.
[3] C. Higman, M. van der Burgt, Gasification, Gulf Publishing, 2008.
[4] A. Kohl, R. Nielsen, Gas Purification, Elsevier, Houston, 1997.
[5] C. Ratnasamy, J.P. Wagner, Catal. Rev. Sci. Eng. 51 (2009) 325–440.
[6] H. Schulz, Appl. Catal. A: Gen. 186 (1999) 3–12.
[7] G.P. Van der Laan, A.A.C.M. Beenackers, Catal. Rev. Sci. Eng. 41 (1999) 255–318.
[8] Studies in Surface Science and Catalysis, Fischer-Tropsch Technology, in: A. Steynberg, M. Dry (Eds.), Elsevier, 2004.
[9] O. Borg, N. Hammer, B.C. Enger, R. Myrstad, O.A. Lindvag, S. Eri, T.H. Skagseth, E. Rytter, J. Catal. 279 (2011) 163–173.
[10] S.S. Pansare, J.D. Allison, Appl. Catal. A: Gen. 387 (2010) 224–230.
[11] W. Torres, S.S. Pansare, J.G. Goodwin, Catal. Rev. 49 (2007) 407–456.
[12] B.S. Turk, T. Merkel, A. Lopez-Ortiz, R.P. Gupta, J.W. Portzer, G. Kishman, B.D. Freeman, G.K. Fleming, Novel Technologies for Gaseous Contaminants Control, US Department of Energy, National Energy Technology Laboratory, 2001.
[13] D. Chiche, C. Diverchy, A.C. Lucquin, F. Porcheron, F. Defoort, Oil Gas Sci. Technol. 68 (2013) 707–723.
[14] O. Shinada, A. Yamada, Y. Koyama, Energy Convers. Manage. 43 (2006) 1221–1233.
[15] D. Vallentin, Energy Policy 36 (2008) 3198–3211.
[16] M.J. Prins, K.J. Ptasinski, F.J.J.G. Janssen, Fuel Process. Technol. 86 (2005) 375–389.
[17] E.M. Jallouli, J.P. Larpin, M. Lambertin, J.C. Colson, Oxid. Met. 11 (1977) 335–354.
[18] M.J.A. Tijmensen, A.P.C. Faaij, C.N. Hamelinck, M.R.N. van Hardeveld, Biomass Bioenergy 23 (2002) 129–152.
[19] M. Asadullah, T. Miyazawa, S.I. Ito, K. Kunimori, M. Yamada, K. Tomishige, Appl. Catal. A: Gen. 267 (2004) 95–102.
[20] A. Demirbas, Energy Convers. Manage. 44 (2003) 1465–1479.
[21] J. Leppälahti, Fuel 74 (1995) 1363–1368.
[22] J. Leppälahti, T. Koljonen, Fuel Process. Technol. 43 (1995) 1–45.
[23] H. Orikasa, A. Tomita, Energy Fuels 17 (2003) 1536–1540.
[24] P. Dagaut, P. Glarborg, M.U. Alzueta, Prog. Energy Combust. Sci. 34 (2008) 1–46.
[25] R. Alvarez-Rodriguez, C. Clemente-Jul, J.A. Martin-Rubi, Fuel 86 (2007) 2081–2089.
[26] F. Frandsen, K. Damjohansen, P. Rasmussen, Prog. Energy Combust. Sci. 20 (1994) 115–138.
[27] A. van der Drift, J. van Doorn, J.W. Vermeulen, Biomass Bioenergy 20 (2001) 45–56.
[28] J. Zhou, S.M. Masutani, D.M. Ishimura, S.Q. Turn, C.M. Kinoshita, Ind. Eng. Chem. Res. 39 (2000) 626–634.
[29] S. Watson, R. Kimmitt, R.B. Rhinesmith, Oil Gas J. 101 (2003) 66–73.
[30] J. Magné-Drisch, J. Gazarian, S. Gonnard, J.-M. Schweitzer, D. Chiche, G. Laborie, G. Perdu, Oil Gas Sci. Technol. 71 (2016) 40.

[31] M. Huisman, The Hydrolysis of Carbonyl Sulfide, Carbon Disulfide and Hydrogen Cyanide on Titania Catalysts PhD Thesis, Utrecht University, The Netherlands, 1994.
[32] P.D.N. Svoronos, T.J. Bruno, Ind. Eng. Chem. Res. 41 (2002) 5321–5336.
[33] C. Rhodes, S.A. Riddel, J. West, B.P. Williams, G.J. Hutchings, Catal. Today 59 (2000) 443–464.
[34] A. Aboulayt, F. Mauge, P.E. Hoggan, J.C. Lavalley, Catal. Lett. 39 (1996) 213–218.
[35] D. Haffad, U. Kameswari, M.M. Bettahar, A. Chambellan, J.C. Lavalley, J. Catal. 172 (1997) 85–92.
[36] S. Tong, I.G. Dalla Lana, K.T. Chuang, Can. J. Chem. Eng. 71 (1993) 392–400.
[37] R. Fiedorow, R. Léauté, I.G. Dalla Lana, J. Catal. 85 (1984) 339–348.
[38] J. West, B.P. Williams, N. Young, C. Rhodes, G.J. Hutchings, Catal. Lett. 74 (2001) 111–114.
[39] P.E. Hoggan, A. Aboulayt, A. Pieplu, P. Nortier, J.C. Lavalley, J. Catal. 149 (1994) 300–306.
[40] B.P. Williams, N.C. Young, J. West, C. Rhodes, G.J. Hutchings, Catal. Today 49 (1999) 99–104.
[41] D.J. Gunn, Chem. Eng. Sci. 42 (1987) 363–373.
[42] F. Yoshida, T. Koyanagi, AIChE J. 8 (1962) 309–316.
[43] E.N. Fuller, J.C. Giddings, J. Chromatogr. Sci. 3 (1965) 222–227.
[44] S. Ergun, A.A. Orning, Chem. Eng. Prog. 48 (1952) 89–94.
[45] D. Handley, P.J. Heggs, Trans. Inst. Chem. Eng. Chem. Eng. 46 (1968) 251–264.
[46] K. Radhakrishnan, A.C. Hindmarsh, NASA Reference Publication 1327 Lawrence Livermore National Laboratory Report UCRL-ID-113855, 1993.
[47] D.W. Marquardt, J. Soc. Ind. Appl. Math. 11 (1963) 431–441.
[48] A. Markovits, J. Ahdjoudj, C. Minot, Surf. Sci. 365 (1996) 649–661.
[49] N.M. Popova, L.A. Sokolova, E.A. Marchenko, L.N. Bobrova, React. Kinet. Catal. Lett. 65 (1998) 363–370.
[50] U. Diebold, Surf. Sci. Rep. 48 (2003) 53–229.
[51] E.W. Thiele, Ind. Eng. Chem. 31 (1939) 916–920.
[52] R.A. Rajadhyaksha, K. Vasudeva, L.K. Doraiswamy, J. Catal. 41 (1976) 61–71.